Nanoscale

Accepted Manuscript

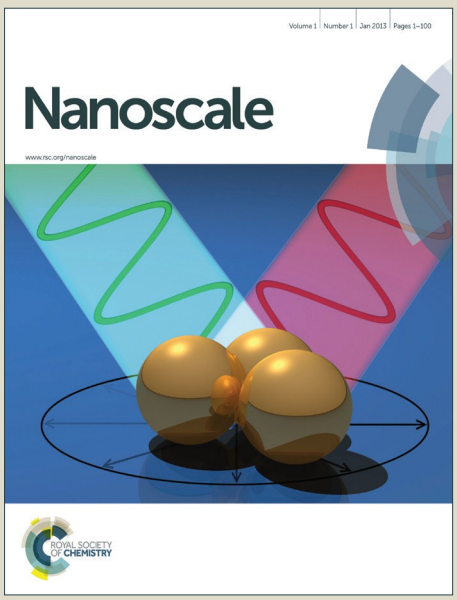

ROYAL SOCIETY OF CHEMISTRY

www.rsc.org/nanoscale

Journal Name

ARTICLE

Hydrogen Storage in Chemical Bond Stabilized Co_9S_8-Graphene Layered Structure

Received 00th January 20xx,
Accepted 00th January 20xx

DOI: 10.1039/x0xx00000x

www.rsc.org/

Wei Qin[a,*], Lu Han[b], Hai Bi[b], Jiahuang Jian[b], Xiaohong Wu[b,*], Peng Gao[c,*]

With the high energy ball milling method, Co_9S_8-decorated reduced graphene oxide (RGO) composite, which shows excellent hydrogen storage capacity, has been successfully fabricated with well-organized layered structure. Moreover, the stabilized mechanism of the well-organized layered structure is investigated and attributed to the strong interactions between Co_9S_8 and defected RGO. The C-S bond interaction is identified and the hydrogen storage process is also studied with different analysis methods. Finally, an optimized Co_9S_8 to RGO weight ratio of 6:1 shows excellent electrochemical performances in terms of the excellent cycle stability and competitive hydrogen storage capacity of 4.86 wt%.

Introduction

The development of hydrogen-based fuel systems requires novel materials which can store large amounts of hydrogen in ambient environment, and at the same time with low weight and small volume[1-3]. Over the past few decades, various solid-state materials have been developed for the hydrogen storage, such as metal alloys[4, 5], metal-organic frameworks[6-8], carbon materials[9, 10], etc. Among these materials, graphene has recently been recognized as one of the most promising candidates for its exceptional mechanical flexibility, good chemical stability and high specific surface area[11]. However, the low binding energy, which is due to physical interaction between molecular hydrogen and graphene, has obstructed the further development for its practical applications in the field of hydrogen storage[12, 13]. Studies have shown that the hydrogen binding energy on graphene can be enhanced by means of metal compound (MC) decorated nanostructure[14, 15]. For instance, MC decorated nanostructured materials can yield higher adsorption energies due to the Kubas interaction[16-18]. However, for the MC-decorated graphene materials, the binding energies of MC atoms with the graphene substrates are less than the cohesive energy in the corresponding bulk MC. Hence, when coated on graphene substrates, MC tends to form agglomerates rather than distribute evenly on the surface of graphene [12, 19]. This usually leads to the collapsed structure of the composites and the resulting decreased electrochemical reversibility and hydrogen storage capacity.

Addressing on these issues, approaches such as wet-chemical route[20], hydrothermal method[21, 22], ultraviolet ozone treatment[23, 24], gentle plasma treatment[25, 26], annealing treatment[27, 28] and high energy ball milling[29-31] have been developed for the purpose of a better correlation of the mixture and at the same time preventing of the MC aggregation effect. Out of those approaches, the high energy ball milling method is favourable for its simple, low-cost, high-yield and environmental friendly properties[32, 33]. This method can not only change the ultimate size of graphene but also introduce lots of lattice defects during fabrication procedure. MC can evenly disperse on the surface of graphene and closely integrates with the active carbon atoms[31, 34]. In some studies, the chemical bonds between the MC and graphene are proposed for stabilizing the layered structure[35]. However, these reports are still short of direct evidence or thorough investigation on the effect of the chemical bond.

In recent years, a series of Co-S compounds have been employed for their excellent hydrogen adsorption capacity and high electrochemical oxidation activity. Amorphous Co-S alloys, processing excellent electrochemical reversibility and high charge-discharge capacity, could be obtained through a ball milling method. Among them, Co_9S_8 has shown very promising performances as energy storage material, such as supercapacitor, solar cell and rechargeable lithium battery materials[36-40]. At the same time, in the electrochemical hydrogen storage process, the disoperation of electrode materials in the high concentration of alkaline electrolyte (6M KOH) has a significant influence on its cycle stability. In the light of these reports, we have carried out detailed studies on fabrication of Co_9S_8 with the high energy ball milling method, which showed a noticeable improvement on the electrochemical hydrogen storage capacities (i.e. 1.79 wt% and 1.19 wt% after 50 cycles). However, only a few reports have addressed on the fabrication of Co_9S_8-decorated graphene

[a] School of Materials Science and Engineering, Harbin Institute of Technology, Harbin, Heilongjiang 150001, PR China. E-mail: qinwei@hit.edu.cn
[b] Department of Chemistry, Harbin Institute of Technology, Harbin, Heilongjiang 150001, PR China. E-mail: wuxiaohong@hit.edu.cn
[c] Harbin Engineering University, Harbin, Heilongjiang 150001, PR China. E-mail: gaopeng@hrbeu.edu.cn
† Footnotes relating to the title and/or authors should appear here.
Electronic Supplementary Information (ESI) available: [details of any supplementary information available should be included here]. See DOI: 10.1039/x0xx00000x

layered structure, and even fewer reports chemical interaction or the framework between Co_9S_8 and graphene.

In this contribution, we report chemical bond stabilized Co_9S_8-graphene layered structure, which prepared with the high energy ball milling method. More importantly, the chemical interaction between Co_9S_8 and graphene is thoroughly investigated together with its hydrogen storage capacity. Compared with the traditional metal decorated graphene, the obtained composites show a much higher electrochemical hydrogen storage capacity and better stability. The chemical interaction of layered structure Co_9S_8-graphene is investigated with different spectral analysis methods. At the same time, the hydrogen storage charge and discharge process of the composite is studied with Land battery system.

Experimental

2.1. Materials

The Co_9S_8 compound is prepared according to the method reported in literature using a FRITSCH PULVERISETTE-7 high energy ball mill[41]. The reduced graphene oxide(RGO) used in this work was purchased from Shen Zhen BRO Nano Technology Co., Ltd.

2.2. Composite preparation

The fabrication procedure and formation mechanism of the layered composite is shown in schematic 1. The Co_9S_8 and RGO were firstly blended together with the weight ratios from 4:1 to 8:1, then ball milling in a ZrO_2 vessel at the speed of 600 rpm for 10h under Ar gas atmosphere. In this process, RGO is crushed into smaller pieces with much more structural defects [31]. Meanwhile, solid Co_9S_8 particles become partially melt during the ball milling process. The resulting Co_9S_8 liquid droplets readily locate on the active site of RGO surface, especially on the defects of RGO. In other word, the uniform Co_9S_8 nanostructures are stabilized and located by the defected RGO. Finally, the Co_9S_8/RGO composite results with the unique layered structure of Co_9S_8 decorated RGO with defects.

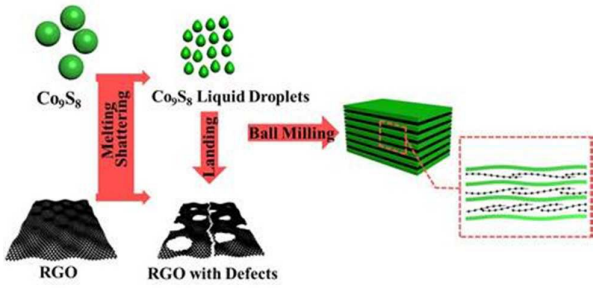

Schematic 1 Illustration of the formation process of Co_9S_8/RGO composite.

2.3. Physical characterization

Fourier transform infrared (FTIR, Nicolet iS10) spectra were recorded using spectrum one in the range 400-4000 cm-1 to characterize the chemical bonds of the samples. X-ray photoelectron spectroscopy (XPS, ESCALAB Mark Ⅱ) with Al Kα X-ray source was performed to analyse the elemental composition of samples. The crystal phases of the samples were analysed by X-ray diffraction (XRD, Rigaku D/max IIIA). Raman spectrum was performed on a confocal Raman spectroscopic system (Jobin Yvon Labram HR800). The morphology, structure and size of the samples were obtained by scanning electron microscopy (SEM, JEOL JSM-6700F) and transmission electron microscopy (TEM, HITACHI H-7000).

2.4. Electrochemical measurements

The electrochemical measurements were carried out similarly as the method reported in previous report[41]. The electrolyte was 6M KOH aqueous solution. The Co_9S_8/RGO negative electrode was charged for 15 h at a current density of 100 mAh g^{-1} and discharged at 30 mAh g^{-1} to 0 V. In order to study the rate capability of samples, the negative electrodes were charged at a current density of 100 mAh g^{-1} for 15 h, and then discharged to 0 V at current density of 200-1000 mAh g^{-1}. All of the electrochemical hydrogen storage experiments were carried out using the battery test system (LAND CT2001A) at room temperature and ambient pressure. The cyclic voltammetry (CV) curves were performed using a three-electrode test cell on electrochemical workstation (PRINCETON PARSTAT 4000).

Results and discussion

We employed FTIR spectroscopy for the investigation of the chemical interaction of the Co_9S_8 decorated RGO (Fig. 1). As for the raw RGO, the band at 1567 and 1200 cm^{-1} are related to the skeletal vibration of the C-C and C-O[31, 42]. The presence of O in RGO should be due to two possible reasons: 1) the oxygen in air is adsorbed and reacts with the as-prepared sample as exposed in air; 2) the oxygen adsorbed on the reactants is introduced into the reaction system. After being decorated by Co_9S_8, the FTIR of the RGO shows remarkable change. Additional peaks related to S-O bending vibration and C-S stretches are clearly identified. The C-O stretching peak at 1200 cm^{-1}, which is observed by the FTIR of the raw RGO, disappears. The C-O-C stretching peak and S-O bending vibration at 1372 cm^{-1} and 1130 cm^{-1} emerge instead[31, 40].

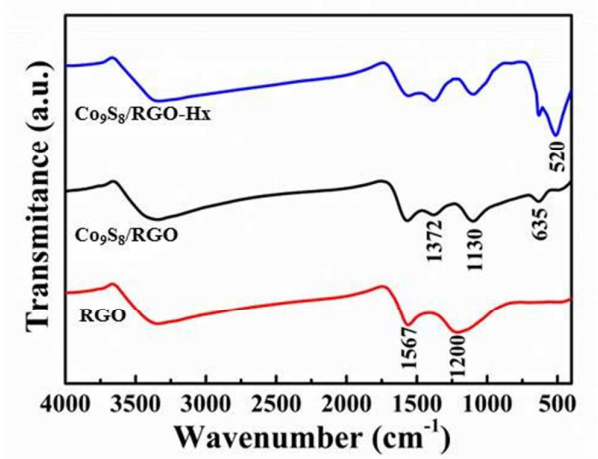

Fig. 1 FTIR spectra of RGO, the original and fully charged Co_9S_8/RGO composite (m_{Co9S8}:m_{RGO} = 6:1).

Journal Name

ARTICLE

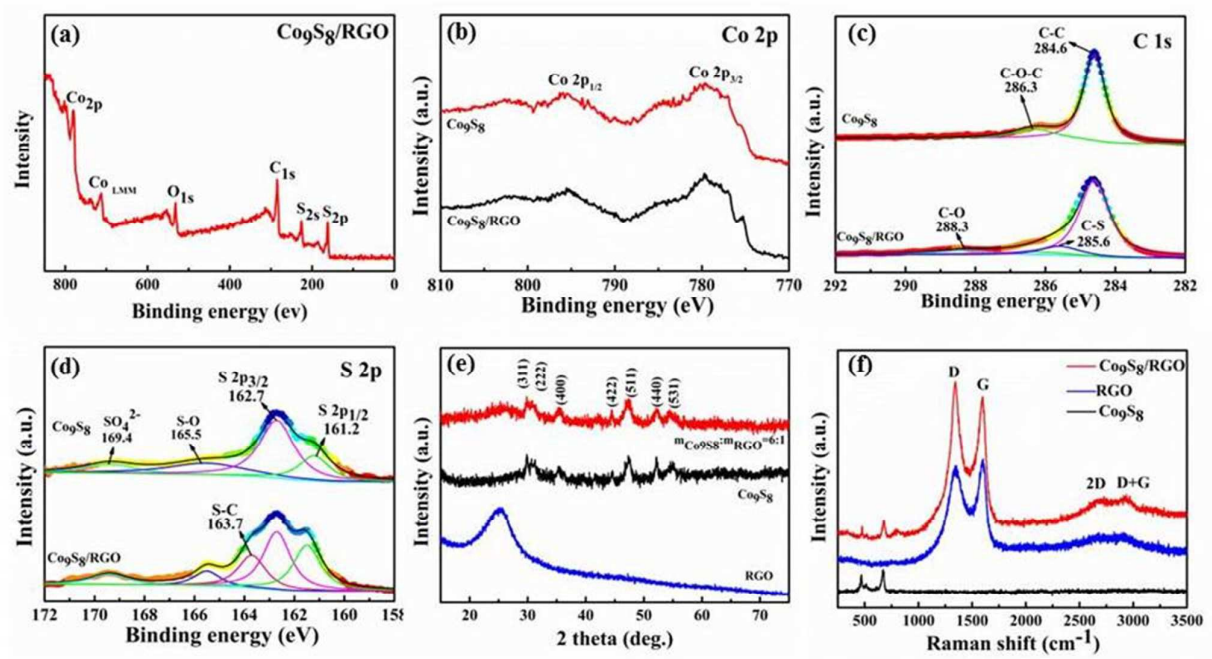

Fig. 2 (a) XPS spectrum of the Co_9S_8/RGO composite; High-resolution (b)Co2p; (c) C1s; (d) S2p XPS spectrum; (e) XRD patterns of raw RGO, Co_9S_8 and the Co_9S_8/RGO composite; (f) Raman spectrum of raw RGO and the Co_9S_8/RGO composite (m_{Co9S8}:m_{RGO} = 6:1).

Importantly, one new characteristic peak at 635 cm^{-1} is identified for the obtained Co_9S_8/RGO composite. When compared with the literature, this peak clearly corresponds to C-S stretches[43, 44]. This result provides definitive proof of the electronic conjugation between Co_9S_8 and RGO. During the ball milling process, the S atoms of the partially melt Co_9S_8 interact with unbounded C atoms at the edge of the defected RGO. As for the fully charged Co_9S_8/RGO composite, the observed FTIR spectrum shows a similar characteristic as for the uncharged one. The footprints of the S-O bending vibration and C-S stretches are still clearly identified. The charging process does not influence the chemical interaction of the Co_9S_8/RGO composite. Besides, one more new peak at 520 cm^{-1} is observed, which corresponds to S-H stretches. This provides definitive proof of a successful hydrogenation. The broad absorption band at 3300 and 3600 cm^{-1} derives from the presence of free hydroxyl groups, which is attributable to bounded water in the KBr.

To explore the interaction of Co_9S_8 and RGO, XPS was used to determine the chemical state. The Co2p, C1s and S2p core levels were recorded for both the Co_9S_8/RGO composite and the precursors. As shown in Fig. 2(a), the XPS peaks at 162.7, 284.6, 460.5, and 530.5 eV are assigned to the binding energies of S2p, C1s, O1s, and Co2p of Co_9S_8/RGO composite, respectively. Fig. 2(b) shows the high-resolution spectra of Co2p in the composite, the peaks at 794.2 and 779.2 eV correspond to the Co2p 1/2 and Co2p 3/2 spin-orbit peaks of cobalt sulfide, which is indeed similar to the situation in Co_9S_8[45]. Each of the spin-orbit peaks (Co2p 1/2 and Co2p 3/2) shows a strong satellite feature at higher binding energy side of the main peak, indicating the formation of octahedrally coordinated, high-spin Co^{2+} ions in cobalt[45, 46]. The shape and peak position, as well as in literature, have no significant change in the spectrum after ball milling, which could provide no information of distinction between different S surroundings of Co[47, 48].

In Fig. 2(c) , the strong peak of C1s at around 284.6 eV can be clearly observed, which corresponds to the sp2 carbon with C-C bonds[49]. Compared to the RGO, the C1s signals become broader for the composite, which suggests an additional component at 285.6 eV This highly characteristic peak should be attributed to the C-S single bonds between the Co_9S_8 and the defected RGO[42]. The small shoulders at 286.3 and 288.3 eV are usually assigned to the formation of C-O and C-O-C bonds, respectively[50].

The S2p peak (Fig. 2(d)) is, for the original Co_9S_8, situated around a large band at 162.7 eV with a strong shoulder at lower binding energy side of the main peak. The broad peak is fitted with two peaks at 162.7 and 161.2 eV respectively, which could be assigned to sulfide cobalt[49]. After ball milling, an additional

shoulder at higher binding energy side of the peak at 162.7 eV is clearly identified. This shoulder is fitted by the peak at 163.7 eV, which corresponds to the presence of S-C bonds[51]. This peak is also identified in the C1s XPS spectrum. Besides the FTIR measurement, the XPS spectrum of the Co_9S_8 decorated RGO provides another strong evidence for the presence of the S-C bond in the layered structure.

XRD patterns were used to examine the overall phases, crystallinity and purity of the precursors and as-prepared composite. As shown in Fig. 2(e), the XRD pattern of the raw RGO has a broad diffraction peak over 20-30°, demonstrating that RGO is non-crystalline. The XRD pattern of Co_9S_8 displays three strong diffraction peaks at 29.8°, 47.6° and 52.1°, respectively, attributed to the pure *fcc* structure (PDF# 02-1459). After high energy ball milling at 600 rpm under Ar atmosphere for 15 hours, the XRD patter of the composite shows that all diffraction peaks corresponding to Co_9S_8 become broadened. In addition, a very weak and broad peak related to RGO is also observed in the XRD pattern of the as-prepared Co_9S_8/RGO composite, indicating RGO in the composite is mostly covered by Co_9S_8.

Raman spectrum is also used to reveal the significant structural changes during the ball milling processing, as shown in Fig. 2(f). The Raman spectra of the samples can be divided into two parts: < 1000 cm^{-1} and >1000 cm^{-1}. Few weak Raman bands (< 1000 cm^{-1}) indexed to Co_9S_8 appeared in the spectrum[52]. The Raman bands after 1000 cm^{-1} are indexed to RGO. For pure RGO, a prominent G band at 1602.13 cm^{-1} is assigned to the vibration of sp2 carbon atoms in an ideal RGO layer and a broad G band at 1354.15 cm^{-1} is associated with sp3 hybridized carbon atoms of RGO from disorder, edges and defects[53]. After ball milling, both G and D bands of Co_9S_8/RGO composite show negative shift to 1595.88 and 1342.54 cm^{-1}, respectively. Moreover, the intensity ratio I_D/I_G of the D to G band increases from 0.94 to 1.01. All the results suggest that the content of the activated carbon atoms in RGO structure from disorder, edges and defects is increased after the high energy ball milling process, which is further confirmed by the shift of the 2D band and D+G band, as well as the increased ratio of I_{D+G}/I_{2D}[54]. Furthermore, our findings suggest that there is a significant reduction in the size of RGO sheets and an accumulation of the defects under mechanical milling impact stress.

In one word, these observations are consistent with the FTIR analysis data and indicate the considerable C-S bonds generated between the interface of RGO and Co_9S_8 by the high energy ball milling process. In general the presence of the C-S bond is identified and served as the constructions for stabilizing the framework of the Co_9S_8 decorated RGO composite. The C-S bonds here provide effective channels for fast ion and electron transport[49]. As shown in the product's examination results of Raman, FTIR and XPS spectrums (Figure 1 and 2), the specific peaks of graphene are residual. So the RGO structure is maintained in the as-prepared sample.

The morphologies and microstructures of the composite were observed by SEM and HTEM. Fig. 3(a) presents a SEM image of the obtained Co_9S_8/RGO composite. It can be seen that the composites exhibit regular layered structures, indicating the mechanochemical functionalization of RGO is efficient. TEM image of the composite is shown in Fig. 3(b). It is obvious that there is a darker region at the centre surrounded by narrow lighter region. The colour difference is due to the element mass difference between Co_9S_8 (darker region) and RGO (lighter region), indicating Co_9S_8 is well dispersion on the surface of RGO. The crystallization of the composite is examined by the SAED results as shown in Fig. 3(b) inset. Typical single-crystal electron diffraction spots and rings appear and show that Co_9S_8 on the surface of RGO sheets is highly crystallinity. HTEM image, as shown in Fig. 3(g), clearly demonstrates the presence of the lattice fringe with spacing of 1.77Å corresponded to the (440) plane of *fcc* Co_9S_8 crystal, in good agreement with the above XRD analysis. To further determine the specific distributions of C, Co and S elements, the corresponding EDS elemental mappings are displayed in Fig. 3(d)–(f). It can be observed that the distributions of C, Co and S are homogeneous throughout the entire Co_9S_8/RGO composite. In sharp contrast, Co and S are concentrated in the centre region. The spatial distributions of C, Co and S further confirm the formation of unique stable layered structure. It should be noted that even after a long time of ultrasonic process during preparation of the TEM specimen, very few RGO sheets are thoroughly exposed, suggesting strong interaction between Co_9S_8 particles and RGO. All the findings suggest that the high energy ball milling process ensures the homogeneous dispersion of Co_9S_8 on the surfaces of RGO to form unique stable layered structure, which is beneficial for the improved electrochemical performances of the resulting composite in the alkaline solution.

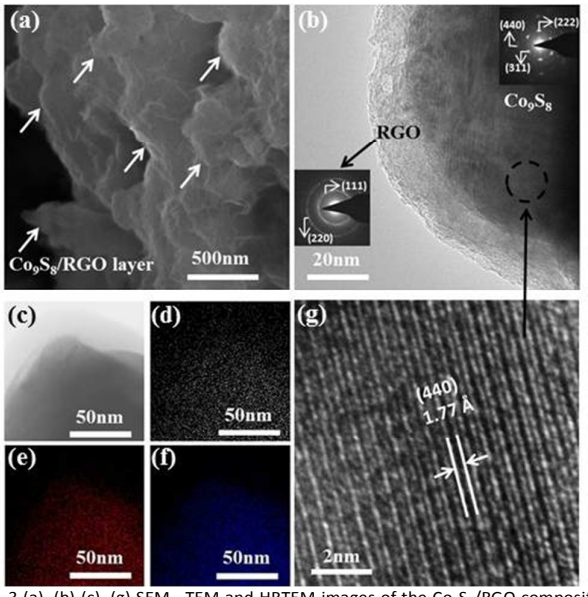

Fig. 3 (a), (b)-(c), (g) SEM , TEM and HRTEM images of the Co_9S_8/RGO composite (m_{Co9S8}:m_{RGO} = 6:1); (d–f) EDS elemental mapping images of C, Co and S in the Co_9S_8/RGO composite.

With the aim of validating the optimized amount of Co_9S_8 in the Co_9S_8/RGO composites, we subsequently measured the corresponding cycle performances at a discharge current density of 30 mA g^{-1} (Fig. 4(a)). The raw RGO in the alkaline

Journal Name

ARTICLE

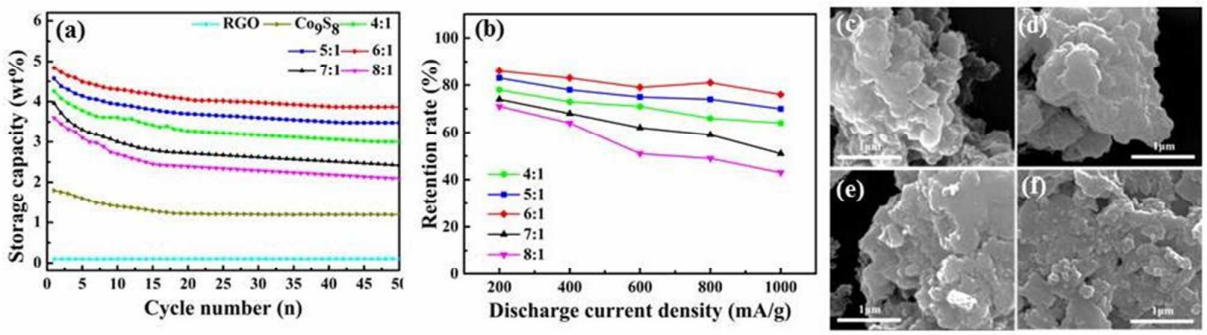

Fig. 4. (a) Cycle performances of raw Co_9S_8, RGO and the Co_9S_8/RGO composites; (b) Rate capabilities of the Co_9S_8/RGO electrodes under various discharge current densities; SEM images of the Co_9S_8/RGO composite with the weight ratios of (c) 4:1; (d) 5:1; (e) 7:1; (f) 8:1.

solution with a capacity of 0.005 wt% is electrochemically inactive, and the capacity of the original Co_9S_8 was 1.79 wt%. The capacities of Co_9S_8/RGO composites increased with increasing Co_9S_8 to RGO weight ratios from 4:1 to 6:1, and the one with m_{Co9S8}:m_{RGO} =6:1 achieved a maximum hydrogen storage capacity as high as 4.86 wt%, which is 2.71 times that of pure Co_9S_8. The corresponding composites electrodes exhibited well capacity retentions, about 80% of the maximum discharge. When the weight ratios rise up to 7:1 and 8:1, the hydrogen storage capacities of the composites decrease remarkably.

In general, all experimental Co_9S_8/RGO composites exhibit the improved electrochemical capacities compared with the raw Co_9S_8 and RGO, which suggesting an activation process during ball milling. In addition, compared with commonly used AB_5 type hydrogen storage materials (i.e. capacity of about 1.27 wt %)[55], the obtained Co_9S_8/RGO composites process much better hydrogen storage capacities. The appropriate mass ratio is to enable the homogeneous dispersion of the Co_9S_8 on the surface of RGO, which is required for the higher capacities. During the high energy ball milling process, the particle sizes of the original Co_9S_8 significantly decrease; the efficient surface areas of Co_9S_8 increase to provide more contact areas with the alkaline solution, which is beneficial for the subsequent surface electrochemical hydrogenation reactions. The C-S bond ensures a stable layered structure of the composite and at the same time offers electron transfer channel between the Co_9S_8. Moreover, the generated hydrogen can store efficiently in between the framework. If the Co_9S_8 to RGO weight ratios higher than 7:1 in the composites, the hydrogen storage capacities of the composites decrease. As shown in Fig. 4(e) and (f), the defected RGO is not enough to stabilize all of the Co_9S_8 particles. The Co_9S_8 particles tend to agglomerate, and in some degree cause the partially corruptions of the framework. The obtained Co_9S_8 nanoparticles are stabilized by the RGO with the help of the C-S bond. The appropriate mass ratio is to enable the homogeneous dispersion of the Co_9S_8 on the surface of RGO.

Moreover, the fraction of RGO in the composites could be required for the stability of the resulting electrode, as indicated by the fact that the cycle performance of the composites electrodes with is almost same as that of the pure Co_9S_8 electrode.

Fig. 4(b) gives the rate capabilities of Co_9S_8/RGO electrodes under different current densities: 200, 400, 600, 800 and 1000 mA g^{-1}. It can be seen that the reversible discharge capacities have different decline trends with increasing the current density, which is consistent with the previous findings. When the weight ratios lower than 6:1, the electrodes exhibit better retention rates with the current density incensement. These are due to the flexibility of RGO and formation of the C-S bonds, which can buffer the volume changes during the charge-discharge process.

As a result, the unique layered structure of Co_9S_8/RGO composite effectively prevents the aggregation of Co_9S_8 and consequently provides more hydrogen adsorption sites, which is favourable for effective hydrogen storage and retention capacities. The composite with Co_9S_8 to RGO weight ratio of 6:1 shows the optimized properties in terms of the best discharge capacity and cycle stability, therefore, it was selected for following investigations about other electrochemical performances.

To explore the electrochemical reaction process and mechanism of Co_9S_8/RGO composite during hydrogen storage, the charge-discharge curves were recorded at a discharge current density of 30 mAh g^{-1}, as shown in Fig. 5(a). The discharge process corresponds to the H_2 relaxation process. The hydrogen storage capability is calculated according to the hydrogen stored release out the layered structure. As can be seen, the charging voltage plateau appeared at about 1.40 V, which can be attributed to the reaction of Co_9S_8/RGO→Co_9S_8/RGO-Hx. The composite has three

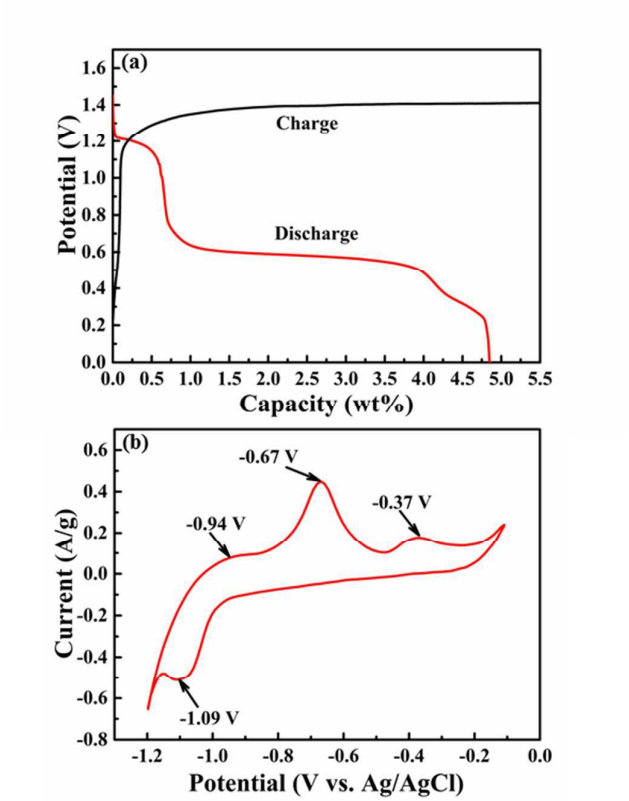

Fig.5. (a) Charge-discharge curves and (b) Cyclic voltammogram curves of the Co_9S_8/RGO composite (m_{Co9S8}:m_{ROG} = 6:1).

discharging voltage plateaus, and the discharge capacity is about 4.86 wt%, which corresponding to the hydrogen storage capability. According to the XRD patterns of the discharged Co_9S_8/RGO composite (Fig.S5), the composition of the layered structure remains the same during the charging and discharging process.

To explore the electrochemical hydrogen adsorption-desorption behaviour of Co_9S_8/RGO composite, the cyclic voltammogram (CV) curves for the charge-discharge cycle were recorded as shown in Fig. 5(b). In the cycle, four oxidation and reduction current peaks appear and locate at the potentials of -1.09 V, -0.94 V, -0.67 V and -0.37 V (vs. Ag/AgCl), respectively, corresponding to one charge and three discharge potential plateaus. These indicate that three different hydrogen adsorption sites exist; in other words, there are three different electrochemical hydrogen storage steps in the charging process. The second current peak at about -0.94 V is assigned to the electrochemical oxidation of Co_9S_8/RGO composite, consistent with previous observation[41]. The third potential position at about -0.67 V is attributed to the hydrogen entered into the space sandwiched between the Co_9S_8 and RGO[56]. The last current peak should be related to desorption of hydrogen adsorbed on the surfaces of the composites[37]. The appearance of peaks in the charge and discharge processes further confirm that the reversible electrochemical reaction occurs on Co_9S_8/RGO composites electrode as follows:

Co_9S_8/RGO + xH_2O + $xe^- \leftrightarrow$ Co_9S_8/RGO-Hx + xOH^-

Conclusions

In summary, the C-S bond interaction between the Co_9S_8 and the defected RGO is achieved and thoroughly investigated for the first time. The bond, identified here, successfully supports and stabilizes layered structure. With this unique layered structure, excellent hydrogen storage capability has been achieved by the Co_9S_8 decorated RGO composite.

The bond not only prevents Co_9S_8 nanoparticles from aggregating, but also provides effective channels for fast ion and electron transport. The RGO in this system acts as a conducting coating on Co_9S_8, which not only significantly enhances the electrical conductivity of the material, but also supplies continuous conductive paths between Co_9S_8 particle and RGO sheets. Last but not least, each of the spaces between the RGO sheets, provides elastic buffer spaces to accommodate the volume changes during hydrogen insertion and extraction, which attributes to excellent cyclability and high rates retention ability. In one word, we report the importance of the C-S bond for the hydrogen storage capability of the Co_9S_8 decorated RGO, and highlight the way of the fabrication of MC decorated RGO with chemical bond stabilized layered structure.

Acknowledgements

This work was supported by the National Natural Science Foundation of China (No. 51173033; No. 51572060; No. 51502062), the Fundamental Research Funds for the Central Universities (No. HIT.BRETIII. 201224 and 201312), and Excellent Youth Foundation of Heilongjiang Scientific Committee (No. JC2015010).

Notes and references

1.S. Ott, *Science*, 2011, 333, 1714-1715.
2.W. Lei, H. Zhang, Y. Wu, B. Zhang, D. Liu, S. Qin, Z. Liu, L. Liu, Y. Ma and Y. Chen, *Nano Energy*, 2014, 6, 219-224.
3.H. Lee, J.-w. Lee, D. Y. Kim, J. Park, Y.-T. Seo, H. Zeng, I. L. Moudrakovski, C. I. Ratcliffe and J. A. Ripmeester, Nature, 2005, 434, 743-746.
4.H. Shao, G. Xin, J. Zheng, X. Li and E. Akiba, *Nano Energy*, 2012, 1, 590-601.
5.H. Emami, K. Edalati, J. Matsuda, E. Akiba and Z. Horita, *Acta Materialia*, 2015, 88, 190-195.
6.H. Deng, C. J. Doonan, H. Furukawa, R. B. Ferreira, J. Towne, C. B. Knobler, B. Wang and O. M. Yaghi, *Science*, 2010, 327, 846-850.
7. K. Sumida, D. Stuck, L. Mino, J. D. Chai, E. D. Bloch, O. Zavorotynska, L. J. Murray, M. Dinca, S. Chavan, S. Bordiga, M. Head-Gordon and J. R. Long, *Journal of the American Chemical Society*, 2013, 135, 1083-1091.
8. N. L. Rosi, J. Eckert, M. Eddaoudi, D. T. Vodak, J. Kim, M. O'Keeffe and O. M. Yaghi, *Science*, 2003, 300, 1127-1129.
9. A. C. Dillon, K. M. Jones, T. A. Bekkedahl, C. H. Kiang, D. S. Bethune and M. J. Heben, *Nature*, 1997, 386, 377-379.
10.S. Leyva-Garcia, E. Morallon, D. Cazorla-Amoros, F. Beguin and D. Lozano-Castello, *Carbon*, 2014, 69, 401-408.

11.K. S. Novoselov, A. K. Geim, S. V. Morozov, D. Jiang, Y. Zhang, S. V. Dubonos, I. V. Grigorieva and A. A. Firsov, *Science*, 2004, 306, 666-669.
12.H. Lee, J. Ihm, M. L. Cohen and S. G. Louie, *Nano Letters*, 2010, 10, 793-798.
13.J. S. Bunch, S. S. Verbridge, J. S. Alden, A. M. van der Zande, J. M. Parpia, H. G. Craighead and P. L. McEuen, *Nano Letters*, 2008, 8, 2458-2462.
14.T. Hussain, T. A. Maark, A. De Sarkar and R. Ahuja, *Applied Physics Letters*, 2012, 101.
15.Y. Yu, N. Zhao, C. Shi, C. He, E. Liu and J. Li, *International Journal of Hydrogen Energy*, 2012, 37, 5762-5768.
16.E. D. Simandiras and D. G. Liakos, *Chemical Physics Letters*, 2013, 583, 18-22.
17.A. Reyhani, S. Z. Mortazavi, S. Mirershadi, A. Z. Moshfegh, P. Parvin and A. N. Golikand, *Journal of Physical Chemistry C*, 2011, 115, 6994-7001.
18.G. J. Kubas, R. R. Ryan, B. I. Swanson, P. J. Vergamini and H. J. Wasserman, *Journal of the American Chemical Society*, 1984, 106, 451-452.
19.Q. Sun, Q. Wang, P. Jena and Y. Kawazoe, *Journal of the American Chemical Society*, 2005, 127, 14582-14583.
20.L. Xing, C. Cui, C. Ma and X. Xue, *Materials Letters*, 2011, 65, 2104-2106.
21.Q. Wang, J. Zhao, W. Shan, X. Xia, L. Xing and X. Xue, *Journal of Alloys and Compounds*, 2014, 590, 424-427.
22.Q. Wang, C.-Y. Zhang, W.-F. Shan, L.-L. Xing and X.-Y. Xue, *Materials Letters*, 2014, 118, 66-68.
23.W. Li, Y. R. Liang, D. M. Yu, L. M. Peng, K. P. Pernstich, T. Shen, A. R. H. Walker, G. J. Cheng, C. A. Hacker, C. A. Richter, Q. L. Li, D. J. Gundlach and X. L. Liang, *Applied Physics Letters*, 2013, 102.
24.Y. Mulyana, M. Horita, Y. Ishikawa, Y. Uraoka and S. Koh, *Applied Physics Letters*, 2013, 103.
25.J. A. Robinson, M. LaBella, M. Zhu, M. Hollander, R. Kasarda, Z. Hughes, K. Trumbull, R. Cavalero and D. Snyder, *Applied Physics Letters*, 2011, 98.
26.D. W. Yue, C. H. Ra, X. C. Liu, D. Y. Lee and W. J. Yoo, *Nanoscale*, 2015, 7, 825-831.
27.W. S. Leong, C. T. Nai and J. T. L. Thong, *Nano Letters*, 2014, 14, 3840-3847.
28.C. E. Malec, B. Elkus and D. Davidović, *Solid State Communications*, 2011, 151, 1791-1793.
29.J. Ambrosio-Martin, G. Gorrasi, A. Lopez-Rubio, M. J. Fabra, L. C. Mas, M. A. Lopez-Manchado and J. M. Lagaron, *J. Appl. Polym. Sci.*, 2015, 132.
30.S. Li, M. Ling, J. X. Qiu, J. S. Han and S. Q. Zhang, *Journal of Materials Chemistry A*, 2015, 3, 9700-9706.
31.I.-Y. Jeon, Y.-R. Shin, G.-J. Sohn, H.-J. Choi, S.-Y. Bae, J. Mahmood, S.-M. Jung, J.-M. Seo, M.-J. Kim, D. W. Chang, L. Dai and J.-B. Baek, *Proceedings of the National Academy of Sciences of the United States of America*, 2012, 109, 5588-5593.
32.S. Yang, P. Gao, D. Bao, Y. Chen, L. Wang, P. Yang, G. Li and Y. Sun, *Journal of Materials Chemistry A*, 2013, 1, 6731-6735.
33.P. Gao, Y. Wang, S. Yang, Y. Chen, Z. Xue, L. Wang, G. Li and Y. Sun, *International Journal of Hydrogen Energy*, 2012, 37, 17126-17130.
34.Y. Cui, L. D. Wang, B. Li, G. J. Cao and W. D. Fei, *Acta Metall. Sin.-Engl. Lett.*, 2014, 27, 937-943.
35.D. Bao, P. Gao, X. Shen, C. Chang, L. Wang, Y. Wang, Y. Chen, X. Zhou, S. Sun, G. Li and P. Yang, *Acs Applied Materials & Interfaces*, 2014, 6, 2902-2909.
36.J. Xu, Q. F. Wang, X. W. Wang, Q. Y. Xiang, B. Hang, D. Chen and G. Z. Shen, *Acs Nano*, 2013, 7, 5453-5462.
37.R. C. Jin, J. H. Zhou, Y. S. Guan, H. Liu and G. Chen, *Journal of Materials Chemistry A*, 2014, 2, 13241-13244.
38.W. X. Guo, C. Chen, M. D. Ye, M. Q. Lv and C. J. Lin, *Nanoscale*, 2014, 6, 3656-3663.
39.Y. L. Zhou, D. Yan, H. Y. Xu, S. Liu, J. Yang and Y. T. Qian, *Nanoscale*, 2015, 7, 3520-3525.
40.R. Ramachandran, M. Saranya, C. Santhosh, V. Velmurugan, B. P. C. Raghupathy, S. K. Jeong and A. N. Grace, *Rsc Advances*, 2014, 4, 21151-21162.
41.W. Qin, B. Hu, D. Bao and P. Gao, *International Journal of Hydrogen Energy*, 2014, 39, 9300-9306.
42.A. S. Sarac, *Microelectronic Engineering*, 2006, 83, 1534-1537.
43.W. L. Qian and S. Krimm, *Biopolymers*, 1992, 32, 1503-1518.
44.V. Arjunan, A. Raj, P. Ravindran and S. Mohan, *Spectrochimica Acta Part A: Molecular and Biomolecular Spectroscopy*, 2014, 118, 951-965.
45.J. G. Kim, D. L. Pugmire, D. Battaglia and M. A. Langell, *Applied Surface Science*, 2000, 165, 70-84.
46.S. C. Petitto, E. M. Marsh, G. A. Carson and M. A. Langell, *Journal of Molecular Catalysis A: Chemical*, 2008, 281, 49-58.
47.T. Fix, M. Liberati, H. Aubriet, S. L. Sahonta, R. Bali, C. Becker, D. Ruch, J. L. MacManus-Driscoll, E. Arenholz and M. G. Blamire, *New Journal of Physics*, 2009, 11.
48.C. Loussot, P. Afanasiev, M. Vrinat, H. Jobic and P. C. Leverd, *Chemistry of Materials*, 2006, 18, 5659-5668.
49.K. Dai, D. Li, L. Lu, Q. Liu, J. Lv and G. Zhu, *Rsc Advances*, 2014, 4, 29216-29222.
50.V. M. Mikoushkin, A. S. Kriukov, V. V. Shnitov, A. P. Solonitsyna, V. Y. Fedorov, A. T. Dideykin, D. A. Sakseev, O. Y. Vilkov and V. M. Lavchiev, *Journal of Electron Spectroscopy and Related Phenomena*, 2015, 199, 51-55.
51.J. Sundberg, H. Nyberg, E. Sarhammar, F. Gustavsson, T. Kubart, T. Nyberg, S. Jacobson and U. Jansson, *Surface & Coatings Technology*, 2013, 232, 340-348.
52.L.-L. Feng, G.-D. Li, Y. Liu, Y. Wu, H. Chen, Y. Wang, Y.-C. Zou, D. Wang and X. Zou, *Acs Applied Materials & Interfaces*, 2015, 7, 980-988.
53.S. Kong, Z. Jin, H. Liu and Y. Wang, *Journal of Physical Chemistry C*, 2014, 118, 25355-25364.
54.Z. Sofer, O. Jankovsky, P. Simek, K. Klimova, A. Mackova and M. Pumera, *Acs Nano*, 2014, 8, 7106-7114.
55.J. Y. Kim, C. N. Park, J. S. Shim, C. J. Park, J. Choi and H. Noh, *Journal of Power Sources*, 2008, 180, 648-652.
56.Q. Wang, L. Jiao, H. Du, W. Peng, S. Liu, Y. Wang and H. Yuan, *International Journal of Hydrogen Energy*, 2010, 35, 8357-8362.